

First-principles study on Small Polaron and Li diffusion in layered LiCoO₂

Seryung Ahn¹, Jiyeon Kim^{2,3}, Bongjae Kim⁴, Sooran Kim^{2*}

¹Department of Physics, Kyungpook National University, Daegu 41566, South Korea

²Department of Physics Education, Kyungpook National University, Daegu 41566, South Korea

³The Center for High Energy Physics, Kyungpook National University, Daegu 41566, South Korea

⁴ Department of Physics, Kunsan National University, Gunsan 54150, Korea

* Corresponding author: sooran@knu.ac.kr

Abstract

Li-ion conductivity is one of the essential properties that determine the performance of cathode materials for Li-ion batteries. Here, using the density functional theory, we investigate the polaron stability and its effect on the Li-ion diffusion in layered LiCoO₂ with different magnetic orderings. The localized Co⁴⁺ polaron appears in the magnetic configurations and sets the Li-diffusion barrier of ~0.34 eV. The polaron also migrates in the opposite direction to the Li-diffusion direction. On the other hand, the polaron does not form in the non-magnetic structure, and the Li diffusion barrier without the polaron is 0.21 eV. Although the existence of the polaron increases the diffusion barrier, the magnetically ordered structures are more energetically stable during the migration than the non-magnetic case. Thus, our work advocates the hole polaron migration scenario for Li-ion diffusion. Moreover, we demonstrate that the strong electron correlation of Co ions plays an essential role in stabilizing the Co⁴⁺ polaron.

Introduction

Lithium-ion batteries (LIB) have become key elements as a power source for current portable electronics.¹⁻³ Among various cathode materials for LIBs, layered lithium cobalt oxide, LiCoO₂ is a widely used cathode for rechargeable LIBs with its high energy density and long cyclability.^{4,5} LiCoO₂ as a cathode material was originally suggested by Goodenough in 1980^{6,7} and used in the first commercialized LIB by Sony in 1991.^{2,8} Since then, LiCoO₂ is one of the most extensively studied cathode materials due to its broad use in modern technology revolution and rechargeable battery applications.^{2,4,5}

LiCoO₂ is synthesized at high temperature (~800°C) in a hexagonal layered structure with the space group of $R\bar{3}m$ while it can be synthesized at low temperature (~400°C) in a cubic spinel structure.^{9,10} The layered structure is formed by Co³⁺-based edge-sharing CoO₆ octahedra separated from one another by the Li layer, which is suitable for Li-ion intercalation/deintercalation. Usually, this structure is termed as “O3 structure” where O represents the octahedral site for Li-ion, and the number indicates three types (AB, BC, and CA) of oxygen packing. Stoichiometric LiCoO₂ is in a non-magnetic ground state with low-spin Co³⁺ ions well-explained by ligand field splitting picture.^{11,12} Due to the strong ligand field, Co³⁺ 3d orbitals split into two e_g and fully filled three t_{2g} .¹² The t_{2g} bands further split into a_{1g} and e_g' under trigonal distortion.¹³

When Li is deintercalated in LiCoO₂, previous experimental studies evidenced the existence of Co⁴⁺ charge state in Li_xCoO₂ ($x < 1$).¹³⁻¹⁶ The Co⁴⁺ ion has five 3d electrons and is in a low-spin state (S=1/2) with a half-filled a_{1g} orbital.¹³ Ménétrier *et al.* reported the localized Co⁴⁺ character with the ⁷Li NMR study upon Li deintercalation.¹⁴ Ito *et al.*, also claimed a mixture of $3d^6$ Co³⁺ and $3d^5$ Co⁴⁺ and possible magnetic phase transition at 175 K in Li_xCoO₂ using the temperature dependent magnetic susceptibility study.¹⁵ The photoelectron spectroscopy

investigation suggested the oxidation state change from Co^{3+} to Co^{4+} under the deintercalation of Li.¹⁶ Furthermore, according to the recent soft X-ray spectroscopy by Mizokawa *et al.*,¹³ Co^{3+} with $S=0$ is oxidized to Co^{4+} with $S=1/2$ as the Li-ions are removed. This Co^{4+} state is explained by the polaron picture, where the local lattice distortion and oxygen $2p$ holes are formed around Co^{4+} . These oxygen holes flow back during the Li-ion flow so that they can compensate for the lattice distortion.¹³

Despite the experimental evidence showing localized Co^{4+} or small polaron in Li_xCoO_2 , many Li-ion conductivity studies using first-principles calculations generally do not consider this polaronic effect¹⁷⁻²¹ and only a few papers investigated the polaron diffusion in Li_xCoO_2 .²²⁻²⁵ Most of the local density approximation (LDA) or generalized gradient approximation (GGA) level calculations allow to obtain the Li-ion diffusion barrier without Co^{4+} polaron.^{17,19,24} On the other hand, Hoang *et al.* intensively studied the defect effect in LiCoO_2 using hybrid functional and reported that the defect migration barriers for electron and hole polarons are 0.32 eV and 0.10 eV, respectively.^{22,23} Moradabadi *et al.* presented that the Li-ion diffusion barrier with localized Co^{4+} charge increases about ~ 0.2 eV within the GGA+ U framework.²⁴ While the role of the polaron in LiCoO_2 is gaining attention, the detailed Li-ion diffusion paths along with polaron have not been reported so far to the best of our knowledge. Moreover, Co-ion is a representative $3d$ -transition metal (TM), which is known to show magnetism and strong correlation effect. The role of magnetism and correlation effect on the polaron formation as well as the diffusion process is an essential issue. Thus, it would be worth investigating the interplay of charge, spin, and lattice on Li-ion diffusion in layered Li_xCoO_2 .

In this paper, we have explored the Li-ion/polaron diffusion, electronic properties, and polaron stability in Li_xCoO_2 . Figure 1 illustrates the crystal structure of bulk LiCoO_2 and supercell structure for the delithiated LiCoO_2 . We compare the total energy and Li-diffusion barrier

depending on the magnetic ordering. The magnetic structures with the localized Co^{4+} polaron are more stable than the non-magnetic one without the polaron during the whole diffusion path. It suggests that Li-ion diffusion along with the polaron is more plausible in the actual system than without. When Li-ion migrates with the polaron, the polaron migration path is opposite to the Li-ion one. Furthermore, we discuss the electronic structure of Co^{4+} polaron and the stability of the polaron upon the strength of the electron-electron correlation.

Computational details

All density functional theory (DFT) calculations were carried out using the Vienna *Ab initio* Simulation Package (VASP), which implements the pseudopotential plane wave method.^{26,27} The Perdew-Burke-Ernzerhof generalized-gradient approximation (PBE-GGA) was used for the exchange-correlation functional.²⁸ The PBE+ U calculations were performed to account for the correlated d orbitals of Co-ions, whose effective on-site correlations, $U_{\text{eff}} = U - J$ are 3.4 eV²⁹ unless specified otherwise. The various U_{eff} values (0.0, 1.0, 2.0, 3.0, 4.0, 5.0 eV) and hybrid functional³⁰ are also employed to investigate the effect of electronic correlation on polaron stability in detail. The Heyd-Scueria-Ernzerhof (HSE)06 was used for the hybrid functional with $\alpha=0.25$.³⁰ A plane-wave kinetic energy cutoff is 650 eV for all calculations.

We fully relaxed the hexagonal LiCoO_2 with $R\bar{3}m$ space group and generated $4 \times 4 \times 1$ supercells with two Li vacancies, corresponding to 190 atoms in total as shown in Fig. 1. The composition of the supercell with Li divacancy is $\text{Li}_{0.96}\text{CoO}_2$. We considered both the spin-polarized and non-spin-polarized calculations for the $4 \times 4 \times 1$ supercells. The atomic positions of the $4 \times 4 \times 1$ supercells were optimized until the residual forces were less than 0.01 eV/Å. The nudged elastic band (NEB)^{31,32} method was used to calculate the Li-ion migration barriers with

Li double vacancies. The NEB calculations were converged until the residual force was less than 0.05 eV/\AA . The k -points for the $4 \times 4 \times 1$ supercell were $2 \times 2 \times 2$ and $1 \times 1 \times 1$ for PBE+ U and HSE06 calculations, respectively.

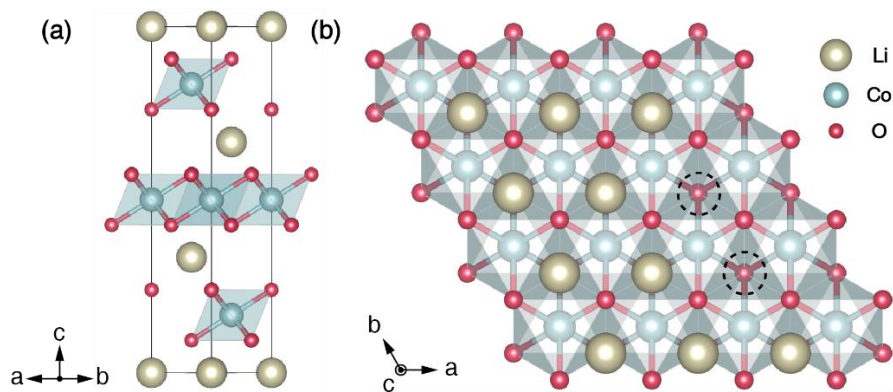


Fig. 1 (a) Crystal structures of bulk layered LiCoO₂ and (b) top view of $4 \times 4 \times 1$ supercell of LiCoO₂ with Li divacancy. The empty circles indicate the position of Li vacancies.

Results and Discussion

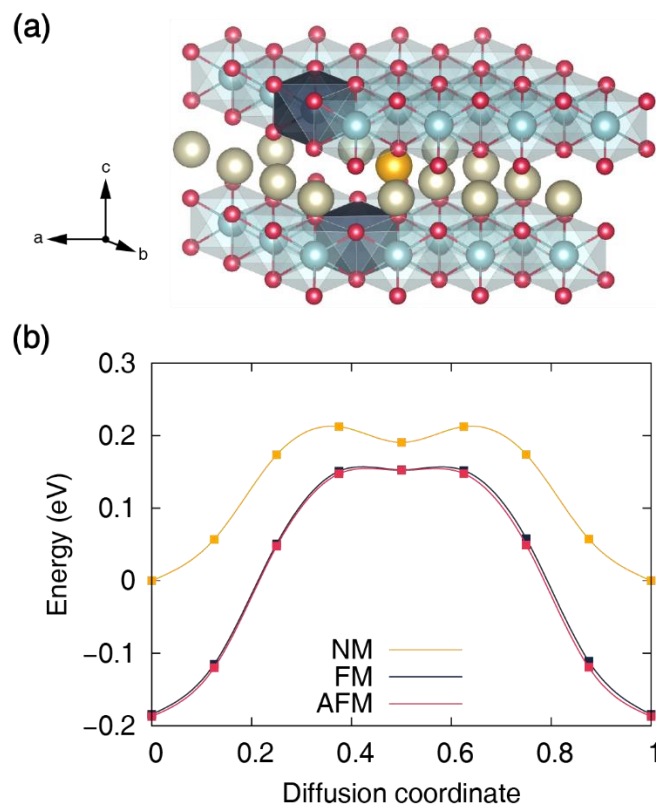


Fig. 2 (a) Polaron formation in LiCoO₂ with Li divacancy. The yellow sphere and darker blue octahedra indicate the moving Li and Co⁴⁺ positions, respectively. (b) Comparison of Li diffusion barriers with and without polaron in different magnetic orderings. Polaron does not localize in non-magnetic (NM) case while the polaron appears in ferro/antiferromagnetic (FM/AFM) structures.

To explore the polaron formation from the localized Co⁴⁺, we relaxed the structures having Li divacancy with different magnetic orderings: non-magnet (NM), ferromagnet (FM), and antiferromagnet (AFM). The spins of two Co⁴⁺ in the FM and AFM structures are in the same and opposite directions, respectively. We found that the polaron forms in magnetic cases only while it does not appear in the NM case. The average lengths of Co³⁺-O bonds in the CoO₆

octahedra were 1.914 Å and 1.927 Å in non-magnetic and magnetic configurations, while the Co⁴⁺-O bond in magnetic structures is 1.894 Å. The contracted TM-O bonds indicate the hole polaron formation. Since the size of the lattice distortion by the localized hole is confined to local Co⁴⁺O₆ octahedra, this type of polaron can correspond to a small polaron.^{33,34} Figure 2(a) illustrates the polaron positions with divacancy: two Co⁴⁺ polarons form and localize near Li vacancies. Co³⁺ is in 3d⁶ electronic configuration with a low spin state, thus only Co⁴⁺ shows significant magnetic moments of 1.000 μ_B with a low spin state in the magnetic structures. The total energy of magnetic cases is ~4 meV/f.u. lower than that of the NM structure, indicating polaron stability. Figure 2 shows the energy difference per 4x4x1 supercell with a Li-ion migration. The energy of FM is only 0.04 meV/f.u. higher than AFM, which suggests the formation of the polaron is local and not very relevant to the magnetic exchanges. The stable polaron from the localized hole in Co⁴⁺O₆ in LiCoO₂ with vacancies is consistent in the previous experiments.¹³⁻¹⁶

Once we identified the polaronic ground of the system, we performed NEB calculations to investigate the effect of polaron on the Li diffusion barrier. Previously, two Li diffusion paths are suggested in layered Li_xCoO₂: one is a single vacancy mechanism through oxygen dumbbell hopping and another is a divacancy mechanism through tetrahedral site hopping.^{17,18,35,36} Because the migration barrier of ~0.2 eV via the divacancy mechanism^{17-19,22} is much lower than that of ~0.4-0.8 eV through the single vacancy mechanism^{17,18,20-22}, lithium diffusion is expected to be predominantly through the divacancy mechanism.^{17,18,36} Therefore, we have focused the divacancy model for the Li migration in this work.

Figure 2(b) shows the calculated migration barriers with different magnetic orderings. The energy barriers are 0.212, 0.338, and 0.339 eV for NM, FM, and AFM structures, respectively. The Li diffusion barrier of the NM case without the Co⁴⁺ polaron agrees well with the previous

Li diffusion barrier of ~ 0.2 eV via the divacancy mechanism.^{17–19,22} When Li-ion diffuses with polaron (FM/AFM cases), the diffusion barrier itself increases about ~ 130 meV, implying that the polaron deteriorates the Li diffusion. In the diffusion coordinates, however, the energy of magnetic structures (FM/AFM) is always lower than that of the NM structure despite a higher diffusion barrier. Therefore, even though the formation of polaron raises the barrier of Li migration, our calculations suggest that Li diffusion involving the polaron migration is energetically favored in Li_xCoO_2 . In addition, the different magnetic ordering does not significantly alter the diffusion barrier as shown in the FM and AFM cases of Fig. 2(b).

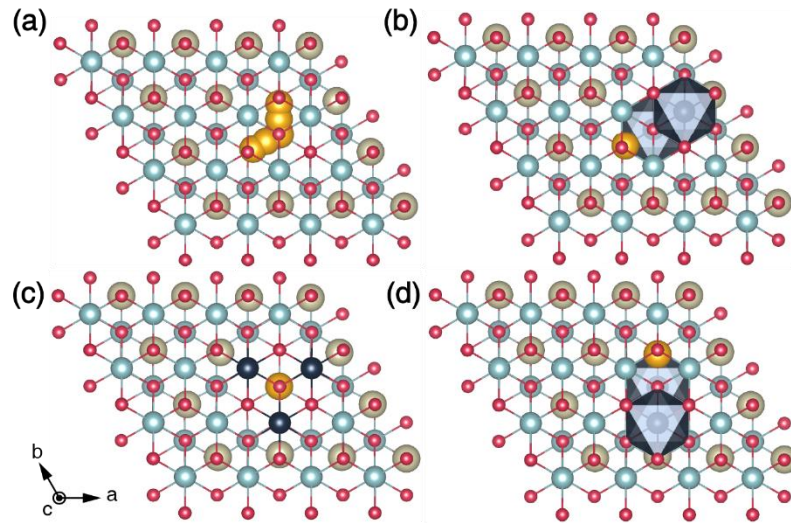


Fig. 3 Li diffusion paths in divacancy mechanism without and with polaron migration. (a) Li migration in the NM structure (b-d) Li and polaron migration in the FM structure. (b), (c) and (d) illustrate the initial, middle, and final atomic configurations, respectively. The transparent polyhedral represents the CoO_6 octahedral with low spin Co^{4+} polaron. The darker blue spheres in (c) indicate Co-ions with a magnetization of $0.148\text{-}0.177 \mu_B$, which is smaller than that of Co^{4+} but larger than that of low spin Co^{3+} .

Figure 3 illustrates the Li diffusion pathways in the NM (without polaron) and FM (with polaron) structures. For the divacancy mechanism^{17,18,35,36}, the Li-ion migrates from one octahedral site to a neighboring octahedral site through the tetrahedral site as shown in Fig. 3(a). On the other hand, when both Li-ion and Co⁴⁺ polaron diffuse, the diffusion directions are opposite. There are two polarons near Li-vacancies: one is above the Li layer with the vacancy, and another is below the Li layer. As shown in Fig. 3(b) and (d), when Li-ion migrates upwards in Fig. 3(b-d), one polaron migrates downwards. Another polaron below migrating Li-ion keeps its position and does not migrate. These opposite directions of Li/polaron diffusions agree well with Li-ion flow with the oxygen hole surrounding Co⁴⁺ backflow.¹³

When Li-ion is at the tetrahedral site in the diffusion path, the polarons are delocalized as in Fig. 3(c): instead of two Co⁴⁺ polarons with the magnetization of 1.000 μ_B , three Co^{3.x+} appear with the magnetization of 0.148, 0.159 and 0.177 μ_B . In addition, the Li and polaron diffusions in the AFM ordering are the same as the FM case, suggesting the energy scale involved in the polaron formation and lattices are much larger than the magnetic exchanges.

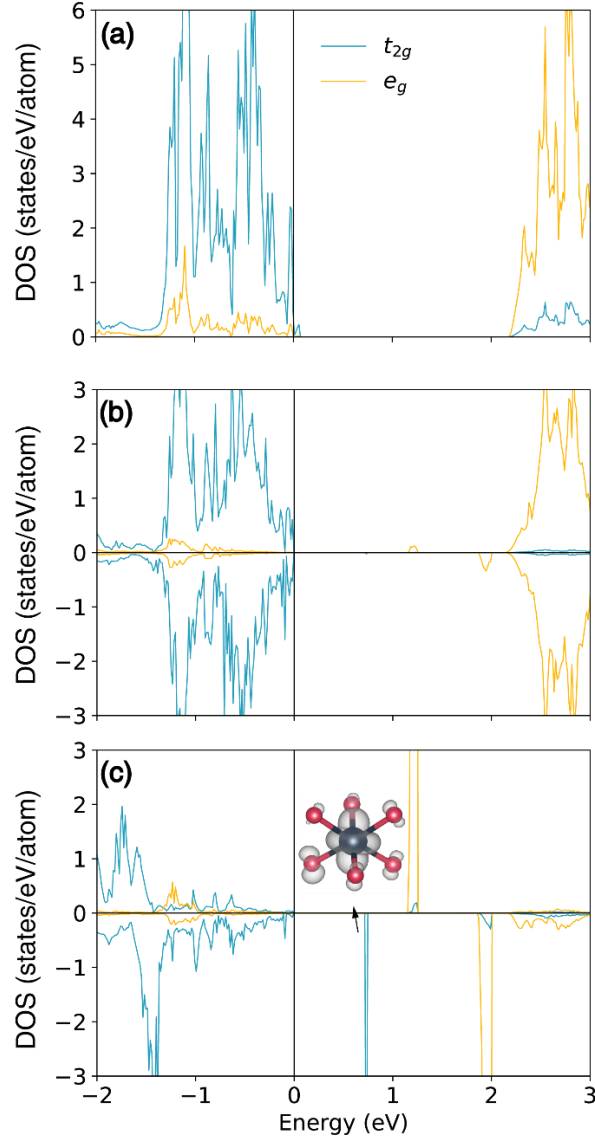


Fig. 4 Projected density of states (PDOS) of $3d$ orbitals of (a) Co-ion in the NM structure. (b) Co^{3+} , and (c) Co^{4+} in the FM structure. (Inset) Charge density isosurface of CoO_6 octahedral t_{2g} hole band.

Now, we look further into electronic structures. We have calculated the projected density of states (PDOS) of the Co $3d$ orbitals in the NM and FM structures as in Fig. 4. For the NM structure, t_{2g} bands are mostly occupied while e_g bands are unoccupied, which indicate the low spin state of Co-ion. The DOS of Co ion in the NM case is almost the same as that of Co^{3+} in the FM case except for a slight hole state of t_{2g} orbital near the Fermi level. These t_{2g} hole bands

originate from the Li divacancy oxidizing Co-ions overall, which results in the metallic phase.

The FM structure shows a clear separation between Co^{3+} (Fig. 4(b)) and Co^{4+} (Fig. 4(c)). The six electrons of Co^{3+} fully occupy the t_{2g} triplet with the low spin state while five electrons of Co^{4+} generate hole bands in t_{2g} bands with the magnetic moment of $1.000 \mu_B$. The FM structure exhibits the insulating phase with a band gap of 0.72 eV. The band gap arises from the gap between t_{2g} orbitals of Co^{4+} ion as shown in Fig. 4(c). In the case of Co^{4+} , the unoccupied e_g exhibits two peaks and part of t_{2g} becomes one unoccupied peak. The inset of Fig. 4(c) illustrates the charge density of the unoccupied $\text{Co}^{4+} t_{2g}$ orbital. The charge density indicates that the unpaired electrons are located at the a_{1g} orbital, which is consistent with the previous studies.^{13,37} Furthermore, we performed the Bader charge analysis on oxygens around Co^{3+} and Co^{4+} , and the average charges of oxygen atoms are 7.064 and 6.982, respectively. The smaller oxygen Bader charge around Co^{4+} than that of Co^{3+} indicates the oxygen hole bounded around Co^{4+} , which agrees well with the previous experiments.^{13,38} The charge density in Fig. 4(c) also shows the oxygen hole around Co^{4+} . In addition, the electronic structure of the AFM structure is similar to that of the FM case.

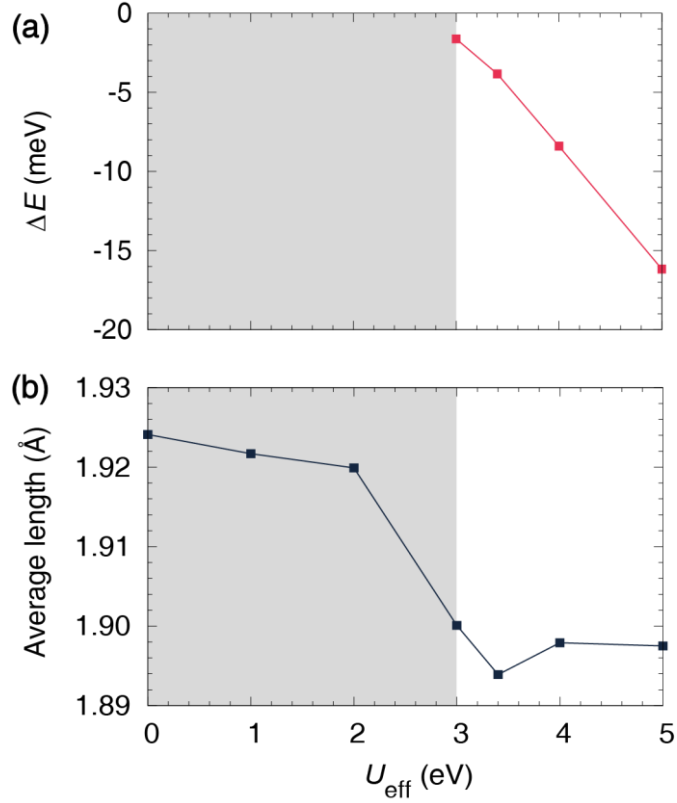


Fig. 5 Polaron stability depending on the electron correlation. (a) The energy difference between polaron and non-polaron structures per formula unit and (b) Average Co-O bond length of CoO_6 as a function of U_{eff} . The gray shaded area represents where the Co^{4+} polaron is not stabilized.

The formation and behaviors of polarons, especially, at the TM-ion sites, are known to largely depend on the degree of the localization of the electron charges. Hence, the strength of the electron-electron correlation, the so-called U , plays an important role in polaron stability. For this, we have studied the role of the U within the DFT+ U scheme on the stability of the polaronic ground by calculating the energy difference, ΔE between polaron and non-polaron structures and average Co-O bond length of Co^{4+} octahedra as a function of U_{eff} from 0 to 5 eV. Figure 5(a) shows that the Co^{4+} polaron starts to be stable when U_{eff} is larger than 3 eV and the

magnitude of ΔE increases as the U_{eff} increases. This shows that a sizable correlation effect is essential for polaron formation, and the critical U_{eff} for the polaron formation is 3eV. Note that the usual U_{eff} values employed for Co^{3-4+} is about $\sim 3-6$ eV.^{19,30,39,40} We further performed the hybrid HSE06 functional calculation, which is known to include the longer-range Hartree-Fock exchange and effective for the description of the polaron. We found that the magnitude of ΔE becomes larger with the hybrid functional whose ΔE is -22.9 meV/f.u.. The HSE calculations also suggest the well-stabilized small polaron in Li_xCoO_2 .

Figure 5(b) shows the average length of Co-O in the octahedra depending on the U_{eff} . When U_{eff} is larger than 3eV, the average length is significantly reduced, which indicates the polaron formation. Although the magnitude of ΔE becomes larger with increasing U_{eff} , the average length does not notably change after $U_{\text{eff}}=3\text{eV}$. It suggests that the increased magnitude of ΔE with $U_{\text{eff}} > 3\text{eV}$ originates from the electronic part rather than lattice deformation.

Conclusions

In conclusion, we demonstrate that the interplay of magnetic ordering and strong Coulomb correlation can affect the polaron formation and Li-ion diffusion using first-principles calculations. The Co^{4+} polaron only appears with the FM/AFM magnetic structure while the NM one does not exhibit the polaron. We have found that the existence of polaron increases the diffusion barrier, but decreases the total energy compared to the energy without the polaron formation. Therefore, we expect that the actual Li migration occurs with the polaron. While Li-ion diffuses, the polaron also migrates whose direction is opposite to the direction of Li diffusion. Furthermore, we show that the strong electron correlation of Co- d orbital stabilizes the polaron formation. We hope that this study can stimulate the detailed investigation of the

alkali-ion diffusion under various conditions such as magnetic ordering, strong electronic correlation, and lattice deformation for Li/Na-ion cathode materials.

Conflicts of interest

There are no conflicts to declare

Acknowledgements

We thank the fruitful discussion with Dr. Kyung-Tae Ko. This work was supported by the National Research Foundation of Korea (NRF) (Grant No. 2022R1F1A1063011, 2021R1C1C1007017), KISTI Supercomputing Center (Project No. KSC-2021-CRE-0495, KSC-2021-CRE-0605). S.K and B.K thank the hospitality of the PCS at IBS, Daejeon, Korea (IBS-R024-D1). BK acknowledges support from the Korea Institute of Energy Technology Evaluation and Planning (KETEP) grant funded by the Korea government (MOTIE) (20224000000220, Jeonbuk Regional Energy Cluster Training of human resources).

References

- 1 M. Armand and J. M. Tarascon, *Nature*, 2008, **451**, 652–657.
- 2 J.-M. Tarascon and M. Armand, *Nature*, 2001, **414**, 359–367.
- 3 M. S. Whittingham, *MRS. Bull.*, 2008, **33**, 411–419.
- 4 Y. Lyu, X. Wu, K. Wang, Z. Feng, T. Cheng, Y. Liu, M. Wang, R. Chen, L. Xu, J. Zhou, Y. Lu and B. Guo, *Adv. Energy. Mater.*, 2021, **11**, 2000982–201010.
- 5 C. Daniel, D. Mohanty, J. Li and D. L. Wood, *AIP Conf. Proc.*, 2014, **1597**, 26–43.
- 6 K. Mizushima, P. C. Jones, P. J. Wiseman and J. B. Goodenough, *Mat. Res. Bull.*, 1980, **15**, 783–789.
- 7 J. B. Goodenough, K. Mizushima and T. Takeda, *Jpn. J. Appl. Phys.*, 1980, **19**, 305–313.
- 8 Y. Nishi, *J. Power Sources*, 2001, **100**, 101–106.
- 9 E. Rossen, J. N. Reimers and J. R. Dahn, *Solid State Ion.*, 1993, **62**, 53–60.
- 10 E. Antolini, *Solid State Ion.*, 2004, **170**, 159–171.
- 11 J. van Elp, J. L. Wieland, H. Eskes, P. Kuiper, G. A. Sawatzky, F. M. F. de Groot and T. S. Turner, *Phys. Rev. B*, 1991, **44**, 6090–6103.
- 12 M. T. Czyzyk, R. Potze and G. A. Sawatzky, *Phys. Rev. B*, 1992, **46**, 3729–3736.

- 13 T. Mizokawa, Y. Wakisaka, T. Sudayama, C. Iwai, K. Miyoshi, J. Takeuchi, H. Wadati, D. G. Hawthorn, T. Z. Regier and G. A. Sawatzky, *Phys. Rev. Lett.*, 2013, **111**, 056404–056408.
- 14 M. Ménétrier, I. Saadoune, S. Lévassieur and C. Delmas, *J. Mater. Chem.*, 1999, **9**, 1135–1140.
- 15 A. Ito, K. Tanaka, H. Kawaji, T. Atake, N. Ando and Y. Hato, *J. Therm. Anal. Cal.*, 2008, **92**, 399–401.
- 16 S. Laubach, S. Laubach, P. C. Schmidt, D. Enslin, S. Schmid, W. Jaegermann, A. Thißen, K. Nikolowski and H. Ehrenberg, *Phys. Chem. Chem. Phys.*, 2009, **11**, 3278–3289.
- 17 A. Van der Ven and G. Ceder, *Electrochem. Solid-State Lett.*, 2000, **3**, 301–304.
- 18 A. Van der Ven and G. Ceder, *J. Power Sources*, 2001, **97**, 529–531.
- 19 S. P. Ong, V. L. Chevrier, G. Hautier, A. Jain, C. Moore, S. Kim, X. Ma and G. Ceder, *Energy Environ. Sci.*, 2011, **4**, 3680–3688.
- 20 B. Andriyevsky, K. Doll and T. Jacob, *Phys. Chem. Chem. Phys.*, 2014, **16**, 23412–23420.
- 21 F. Ning, S. Li, B. Xu and C. Ouyang, *Solid State Ion*, 2014, **263**, 46–48.
- 22 K. Hoang and M. D. Johannes, *J. Mater. Chem. A*, 2014, **2**, 5224–5235.
- 23 K. Hoang and M. D. Johannes, *J. Phys. Condens. Matter*, 2018, **30**, 293001–293022.
- 24 A. Moradabadi and P. Kaghazchi, *Phys. Chem. Chem. Phys.*, 2015, **17**, 22917–22922.
- 25 A. Moradabadi and P. Kaghazchi, *Phys. Rev. Appl.*, 2017, **7**, 064008–064012.
- 26 G. Kresse and J. Furthmüller, *Comput. Mater. Sci.*, 1996, **6**, 15–50.
- 27 G. Kresse and J. Furthmüller, *Phys. Rev. B*, 1996, **54**, 11169–11186.
- 28 J. P. Perdew, K. Burke and M. Ernzerhof, *Phys. Rev. Lett.*, 1996, **77**, 3865–3868.
- 29 G. Hautier, S. P. Ong, A. Jain, C. J. Moore and G. Ceder, *Phys. Rev. B*, 2012, **85**, 155208–155225.
- 30 A. V. Krukau, O. A. Vydrov, A. F. Izmaylov and G. E. Scuseria, *J. Chem. Phys.*, 2006, **125**, 224106–224111.
- 31 H. Jonsson, G. Mills and K. W. Jacobsen, in *classical and quantum dynamics in condensed phase simulations*, 1998, pp. 385–404.
- 32 G. Henkelman and H. Jónsson, *J. Chem. Phys.*, 2000, **113**, 9978–9985.
- 33 C. Franchini, M. Reticcioli, M. Setvin and U. Diebold, *Nat. Rev. Mater.*, 2021, **6**, 560–586.
- 34 T. Maxisch, F. Zhou and G. Ceder, *Phys. Rev. B*, 2006, **73**, 104301–104306.
- 35 A. Van der Ven, J. Bhattacharya and A. A. Belak, *Acc. Chem. Res.*, 2013, **46**, 1216–1225.
- 36 M. S. Islam and C. A. J. Fisher, *Chem. Soc. Rev.*, 2014, **43**, 185–204.
- 37 F. Xiong, H. J. Yan, Y. Chen, B. Xu, J. X. Le and C. Y. Ouyang, *Int. J. Electrochem. Sci.*, 2012, **7**, 9390–9400.
- 38 W. S. Yoon, K. B. Kim, M. G. Kim, M. K. Lee, H. J. Shin, J. M. Lee, J. S. Lee and C. H. Yo, *J. Phys. Chem. B*, 2002, **106**, 2526–2532.
- 39 F. Zhou, M. Cococcioni, C. A. Marianetti, D. Morgan and G. Ceder, *Phys. Rev. B*, 2004, **70**, 235121–235128.
- 40 B. Kim, K. Kim and S. Kim, *Phys. Rev. Mater.*, 2021, **5**, 035404–035411.

